A Mathematical Interpretation Model of Ti Alloy Micro-Arc Oxidation (MAO) Process and its Experimental Study

Maolin Shi, Hongyou Li

College of Mechanical Engineering and Automation,
Huaqiao University, 668 Jimei rev., Xiamen, Fujian, China, e-mail: shl5985336@126.com

A mathematical interpretation model of micro-arc oxidation process parameters and ceramic coating properties in Ca/P electrolyte system was attempted to establish. The model includes micro-arc oxidation process parameters (power supply voltage U_m, current density J, duty ratio η, electrolyte conductivity and dielectric constant of anodic oxide gas), and the properties of ceramic coating (surface morphology, thickness, pores density, porosity, the average size of pores). The response of current during the process was studied. The properties of ceramic coating (morphologies, thickness and surface statistics) were measured by scanning electron microscopy (SEM), 3-D HIROX video microscope, TT230 coating and layer thickness measuring instrument and image analysis software ImageJx2.0. The current was measured by AC galvanometer GPM-8212. The molar conductivity of NaOH is the highest among the four electrolyte system components, and its concentration has the greatest impact on ceramic coating surface morphology. The analysis agrees with the experimental results in lower concentration (under 0.30 mol/L) extremely. However, there is a discrepancy at higher concentration (0.40 mol/L) since the much more molten metal during the reaction of MAO in higher conductivity electrolyte. Pores density is the major factor in determining the porosity. Current results show that ceramic coating had been generated at 40s under the constant voltage system. The model provides a theoretical base for the interpretation of Ti alloy MAO process and determining the appropriate concentration of NaOH in Ca/P electrolyte system.

Keywords: micro-arc oxidation, Ti alloy, mathematical model, Ca/P electrolyte.

УДК 544.5+544.6

INTRODUCTION

Titanium and its alloys have been widely used for aeronautics, astronautics and dental implants due to their higher strength-to-weight ratio, lower density and superior bio-mechanics compatibility. However, the tribological properties of their surface, corrosion resistance and bio-inert restrict their wider applications. To meet the demand for the properties of industrial and medical applications, micro-arc oxidation (MAO), also commonly called plasma electrolytic oxidation (PEO) [1–3], has been extensively developed to improve the mechanical characters and bioactivity by incorporating SiO_2, Al_2O_3, calcium and phosphorus into TiO_2-based ceramic coating using particular electrolyte systems including particular elements such as Si, Al, Ca or P in the past 40 years from 1970s [4–7]. The TiO_2-based coatings formed on titanium alloys in silicate electrolyte can reduce the friction coefficient significantly, and the ceramic coating in aluminum electrolyte would increase the surface hardness with the promotion of friction performance [7–9]. It is noticed that MAO TiO_2-based coating containing Ca and P which is fabricated in the electrolyte composed of calcium salts such as calcium acetate and calcium dihydrogen phosphate could improve the bioactivity, and its biomedical applications have already received verification and success [10]. That area is likewise the focus area in recent years [11–14].

In the published papers [3–16], researchers have invested in the relationship between the properties of MAO ceramic coating and the process parameters such as species of titanium alloys, electrical parameters and electrolyte components and characters. However, it only forecasts, indicates and demonstrates the “output” (coating properties) based on the “input” (process parameters). The mechanism and reactions (physical, chemical and plasma reactions) during MAO process were concluded as a special word “black box” since the conditions that there are no theoretical models could illuminate the reasons, interpretation and mechanism of the phenomenon and results of MAO process.

Unfortunately, the studies of the establishment of MAO process mechanism depending on the basic theories and statistics of process parameters and its experimental studies were rarely reported. S. Ikonopisov first putted forward a theoretical physical model [17], and Albella proposed the theory of the coating thickness quantitative theory with only a parameter-voltage based on S. Ikonopisov’s model [18]. In recent years, some researchers analyzed the coating structure and its electrical characterization through EIS model, and the simulation results with the current response of experimental samples [19–20].

This paper attempted to establish an electrical mathematical interpretation model to analyze the impact of electrolyte concentration on the MAO

ceramic coating surface morphology, structure, and current response depending on electrochemistry and thermochemistry. In addition, this paper concentrated on the establishment and verification of MAO mathematical electrical interpretation model through MAO experiments in Ca and *P* electrolyte to explain micro-arc oxidation process and provides references to the related researchers.

1. THE DERIVATION AND ESTABLISHMENT OF MAO PROCESS MODEL

1.1. Original establishment of MAO process model

According to the micro-arc oxidation theories from the published references [1–3], [11–15], [19–20], MAO belongs to the category of low temperature plasma in liquid. Electrochemistry and thermalchemistry act a major role in the phase transformation during the whole process [2], [20]. It can be concluded that the sample after MAO is composed of Ti alloy substrate and MAO ceramic coating, which is easily seen in the cross-section morphologies. The main component phases of MAO ceramic coating are anatase and rutile TiO_2 [2], [9–11] Mansfeld [21–22] proposed an equivalent electrical model which specializes in the system of metallic substrate and coating. Y.M. Wang [19] applied EIS model to analyze and simulate the electrical properties of MAO coating, and the results of tests were ideal. Although the coating is composed of porous ceramic coating and dense ceramic coating, after reading other papers about MAO under voltage model and observing our samples, we found that the structure differentiation of MAO coating of voltage model is not as obvious as that of current voltage and even completely indistinct. Therefore, the MAO coating was considered as a whole. Combining Mansfeld model and the actual situation of MAO sample, a promoted model was established after simplifying the experimental conditions as shown in and Fig. 1 and Fig. 2: R_0: resistance of Ti alloy substrate; R_1: resistance of MAO coating; C_1: capacitance of MAO coating. In the process of micro-arc oxidation, a layer of gas generated on the sample surface with obvious capacitance effect. Therefore, C_2 was set to represent the layer of gas. R_s was equivalent resistance of the electrolyte. Figure 2 is the model diagram for micro-arc oxidation process.

Based on the equivalent circuit model shown in Fig. 2, complex impedance Z of ceramic coating could be decided by the equation as below:

$$\frac{1}{Z_1} = \frac{1}{R_1} + j\omega C_1, \tag{1}$$

$$R_1 = \frac{\rho_1(t)d}{A}, \tag{2}$$

$$C_1 = \frac{\varepsilon_1(t)\varepsilon_0' A}{d} \tag{3}$$

j is imaginary unit, ω is input frequency, $\rho_1(t)$ is equivalent resistivity of ceramic coating, and $\varepsilon_1(t)$ is equivalent dielectric constant of ceramic coating, ε_0' is absolute dielectric constant. A and d are sample area and the ceramic coating thickness respectively. It was known that from the published papers:

$$\varepsilon_1(t) = (1-p)\varepsilon_1^{g_1}\varepsilon_2^{g_2} \tag{4}$$

p is porosity, ε_1 and ε_2 are rutile and anatase TiO_2 dielectric constants respectively, g_1 and g_2 are the contents of rutile and anatase TiO_2 $g_1 + g_2 = 1$.

From the electrolyte electrochemical theories and gas capacitance theories, electrolyte resistance and gas capacitance are calculated by formula below:

$$R_2 = \frac{d_e}{c\Lambda_m A}, \tag{5}$$

$$C_2 = \frac{\varepsilon_2(t)\varepsilon_0'' A}{d_{\text{gas}}} \tag{6}$$

d_e and d_{gas} are the thicknesses of electrolyte and anode gas; c is electrolyte concentration; Λ_m molar electrolyte conductivity; $\varepsilon_2(t)$ is relative gas dielectric constant; ε_0'' is absolute dielectric constant.

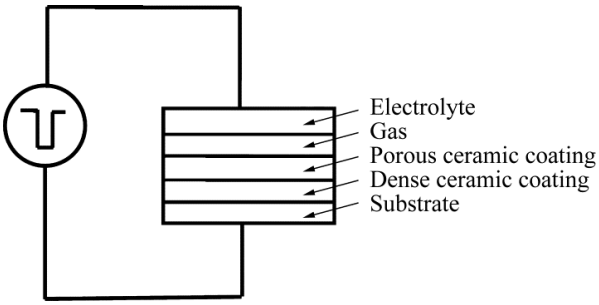

Fig. 1. Model of anodic interface in the process of micro-arc oxidation.

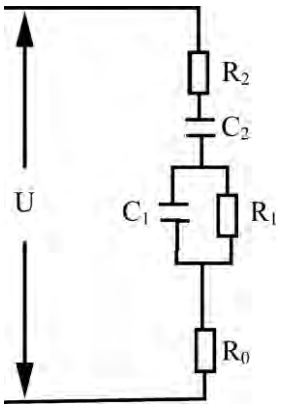

Fig. 2. Electrical model of MAO process.

1.2. Parameter selection

Researchers and scholars who laid the foundation of micro-arc oxidation theories and studied the

experiments and industrial applications share a consensus view that micro-arc oxidation process includes thermal chemical, electrochemical, plasma and other physical or chemical reactions, and TiO_2-based ceramic coating is fabricated on the surface of Ti alloy substrate [2], [7], [21–22]. At the beginning of the whole process, a layer of uneven oxidation with a layer of thin gas on the surface is gene-rated. With time extending, weak thinned area of oxidation layer is breakdown, and the discharge channels form originally. Around the channels, a sharp drop of voltage in an extremely short distance which results in considerable increasing of electrical field strength, and a variety of physical and chemical reactions and ceramic coating is generated. In the process, the electrical properties of the electrolyte and oxidizing gas have important influence, and analyzing the relationship and effect between process parameters and ceramic coating properties is necessary. Combing with equitations 1 ~ 5, the parameters selected as below: electrolyte: molar electrolyte conductivity Λ_m; electrolyte concentration c; anode sample: sample area A; coating thickness d; power: dielectric constant; current I; voltage U.

1.3. Equivalent mathematical model

Depending on the Eq. 1 ~ 5 and complex impedance circuit theories with simplifying and reduction, it can be concluded that the mathematical equivalent electrical model containing the factors with higher influence as follows:

$$|Z| = \frac{\omega R_1^2 C_1}{C_2\left(1+\omega^2 C_1^2 R_1^2\right)} \Big/ \sqrt{2C_1^2 + C_2^2 + 4C_1C_2 + C_1^2R_0^2 + 4R_2^2C_1^2 + 4R_0R_2C_1^2} \tag{7}$$

Eq. 1, 2, 3, 5 & 6 were taken into Eq. 7 (R_0 is almost 0 relatively):

$$|Z| = \frac{\omega \rho_1(t) C_1}{C_2\left(1+\omega^2 C_1^2 R_1^2\right)} \Big/ \sqrt{2(1-p)^2 \varepsilon_1^{2g_1}\varepsilon_2^{2g_2} + \varepsilon_2^2(t)(\varepsilon_0')^2 + 4(1-p)\varepsilon_1^{g_1}\varepsilon_2^{g_2}(t)\varepsilon_0'\varepsilon_0'' + 4\frac{\varepsilon_2^2(t)(\varepsilon_0'')^2 d^2}{c^2\Lambda_m^2 A^2}} \tag{8}$$

From the Eq. 8 as above, it is found that most parameters selected in 2.2 are included. However, current I and voltage U are not. Though the authors' study and some published papers, it is a common view that in voltage system, current response experiences significant change initially and keeps a steady state in the later stage. From the below equations:

$$|Z| = \frac{U}{I}, \tag{9}$$

$$U(t) = \sqrt{\eta} U_m \tag{10}$$

η duty ratio, U_m: voltage amplitude. Eq. 8 is changed as follows:

$$\frac{\sqrt{\eta}U_m}{I} = \frac{\omega \rho_1(t) C_1}{C_2\left(1+\omega^2 C_1^2 R_1^2\right)} \Big/ \sqrt{2\varepsilon_1^2(t)\varepsilon_0^2 + \varepsilon_2^2(t)(\varepsilon_0'')^2 + 4\varepsilon_1(t)\varepsilon_2(t)\varepsilon_0'\varepsilon_0'' + 4\frac{\varepsilon_2^2(t)(\varepsilon_0'')^2 d^2}{c^2\Lambda_m^2 A^2}}. \tag{11}$$

It is seen that micro-arc oxidation process current I, voltage U_m and duty ratio η have an effect on the structure and phase composition. However, most recent studies focus on the phase composition concerning the promoting bioactivity of Ti alloy through MAO, and less attention was paid into the properties and parameters of surface morphologies of MAO coating and their relationship with the process parameters. In this paper, MAO experiments in calcium and phosphorus electrolyte system were operated, and the model above was used to predict and interpret the results of the experiments to verify the feasibility of the mathematical interpretation model. The surface morphologies and surface statistics of MAO ceramic coatings were analyzed specially.

2. EXPERIMENTAL PROCEDURE

2.1. Materials and pre-treatment

In the present work, industrial titanium alloy TB9 with a chemical composition of Ti-3.5Al-8V-6Cr-4Mo-4Zr(at.%) was used as the substrate. The TB9 alloy substrate was machined into rectangular samples with dimension 15 mm × 10 mm × 0.5 mm for MAO process. The samples were polished using 600#, 800#, 1000# and 1200# abrasive paper orderly, and cleaned in distilled water followed by acetone.

2.2. Coating preparation

Micro-arc oxidation coatings were prepared in the electrolyte dissolving reagent-grade chemicals of $Ca(CH_3COO)_2$, NaH_2PO_4, EDTA-2Na and NaOH (the concentration of each component was shown in Table 1) into distilled water. A home-made micro-arc oxidation device (45 Kw) provides the voltages, and the main pulse parameters, such as pulse duration, voltage amplitude and duty cycle were adjusted independently. The electrical parameters were fixed as follows: voltage 250 V, frequency 200 Hz and time 120 s.

Table 1. Electrolyte formula (Unit: mol/L)

No.	$Ca(CH_3COO)_2$	NaH_2PO_4	EDTA-2Na	NaOH
1	0.060	0.040	0.045	0.05
2	0.060	0.040	0.045	0.10
3	0.060	0.040	0.045	0.20
4	0.060	0.040	0.045	0.30
5	0.060	0.040	0.045	0.40

2.3. Coating characterization

The surface and cross-section morphologies were observed by a FEI PHENOM scanning electron mi-

croscopy (SEM) (magnification:2000×&5800×). 3-D images were taken by HIROX video microscope with magnification 2500×. The surface roughness was recorded during the former 3-D testing process. The thickness of MAO coating was determined by TT230 coating and layer thickness measuring instrument.

2.4. Analysis of image

The image from SEM was analyzed by image professional software ImageJx2.0 to achieve porosity, pores density and the average size of pores on MAO coating.Ten positions were selected to collect the statistics about the pores of typical MAO porous structure and calculate the average value in order to keep the data accurate and objective, and so did the thickness.

2.5. Current response measurement

Current response was measured by an AC meter GPM-8212 made in Xiamen China (range: 2.560A; current sensitivity: ± 0.1% at 25□; input resistance: 0.01 Ω) during the experiment. The anode current and cathode current were measured first, and the effective working current was calculated as the final data. After getting the data, Original 8.0 was used to draw the current response curve. The current measurement above was repeated five times and the average value was calculated as the final results.

3. RESULTS AND DISCUSSION

3.1. Properties of ceramic coating morphologies

p (porosity) □ *c* (concentration) can be achieved from Eq. 3, 4&8. In calcium and phosphorus electrolyte system, NaOH concentration acts foremost influence on the electrical characterization and properties of electrolyte among the four components (calcium source salt, phosphorus source salt, complex agent and pH modifier). Therefore, p was predicted to increase with concentration c increasing, and the surface morphology was more poriferous. The experimental results are as follows (Figs. 3 and 4):

From Fig. 3a–e 3-D morphology images, it can be observed that pores are crater shape with lower NaOH concentrations (Fig. 4d and c). When NaOH concentration reaches a certain value, pores are mostly sintered by the melt, and the thickness increases considerably. The first increasing of roughness is a result of the crater shape structure which is the remnant of discharge channels (Fig. 3a to Fig. 3d, Table 2). However, the surface becomes smooth with NaOH concentration continuously increasing, which could be attributed to the mass metallic melt which stacked and coated on the Ti alloy substrate (Table 2). When NaOH concentration are 0.05 mol/L and 0.10 mol/L, the samples morphologies are smooth which is mostly coated by once breakdown melt and appears various micro porous structure; With NaOH concentration increasing until 0.30 mol/L, pores are almost round crater shape with thicker walls, and the amount of pores declines. The pores are repeated breakdown channels. The sample surface changes to be relatively smoother with NaOH 0.40 mol/L, and its porous structure includes round pores and irregular shape ones which were fabricated by coating and discharging during the whole process. Morphologies have no obvious changes in relatively higher concentrations (Fig. 4d and e).

It could be seen that Fig. 4a–c accordance with the model which is established above. Fig. 4d and e with higher concentration have differences and distinctions compared with the deduction conclusion of the established equation. It is mostly because that the amount of melt increased significantly, and it coated and refrigerated on the Ti alloy substrate. The porous structure was fabricated by coating and refrigeration instead of breakdown discharge channels, and its pores' shape is irregular. Thus, the results of higher concentrations shows inconformity with the predicted relationship *p* (porosity) □ *c* (concentration).

3.2. Thickness of MAO coatings

Figure 5 shows the curve of the thickness of MAO coatings depending on NaOH concentration. With NaOH concentration increasing from 0.05 mol/L to 0.40 mol/L, the thickness experiences an upward trend from 4.632 μm to 23.267 μm. However, the thickness curve indicates similar linear variation from 4.632 μm to 9.871 μm under concentration 0.30 mol/L, which is accompanied with the established model in this paper. Related to Figs. 4 and 5, the thickness increasing is ascribed to the effect of melt coating and accumulation. Lower concentration, ceramic coating surface is uneven and rough, and the increasing coating material was mostly brought by the discharges and arcs. Concentration continuously increases until a certain concentration 0.40 mol/L, the material brought by the reactions during the oxidation was enough to coat and accumulate on the original oxidation coating repeatedly. Therefore, the thickness grows up rapidly, and the surface is much smoother.

Combining with Eq. 8&11, concentration c and coating thickness d are directly proportional under the conditions of reacting completely and other parameters keeping stable. From the experimental results as shown above (Figs. 3–5), the curve of the thickness of MAO coatings depending on NaOH concentration reflects better goodness when NaOH concentration is under 0.30 mol/L, which the major of the coating surfaces is mostly composed of the

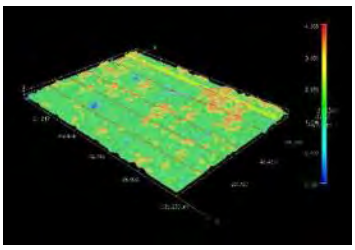

Fig. 3a. Effect of the NaOH concentration on the 3-D morphology (NaOH concentration 0.05 mol/L).

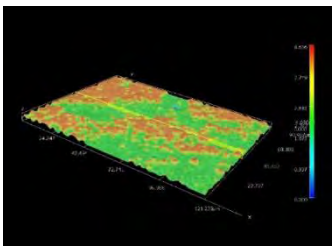

Fig. 3b. Effect of the NaOH concentration on the 3-D morphology (NaOH concentration 0.10 mol/L).

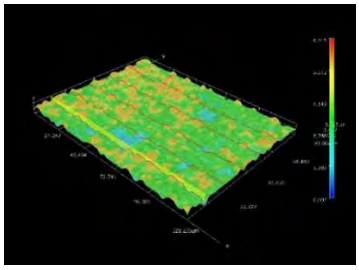

Fig. 3c. Effect of the NaOH concentration on the 3-D morphology (NaOH concentration 0.20 mol/L).

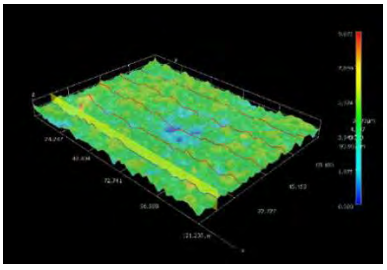

Fig. 3d. Effect of the NaOH concentration on the 3-D morphology (NaOH concentration 0.30 mol/L).

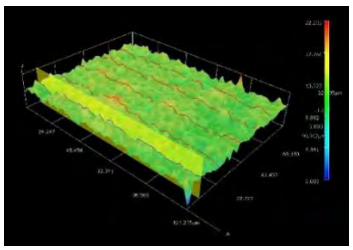

Fig. 3e. Effect of the NaOH concentration on the 3-D morphology (NaOH concentration 0.40 mol/L).

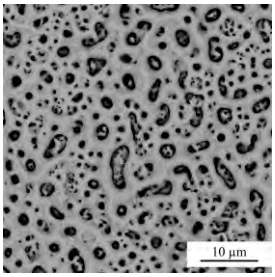

Fig. 4a. Surface morphology of MAO films in electrolytes of different NaOH concentration (NaOH concentration 0.05 mol/L).

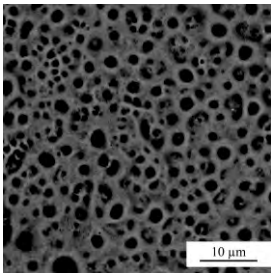

Fig. 4b. Surface morphology of MAO films in electrolytes of different NaOH concentration (NaOH concentration 0.10 mol/L).

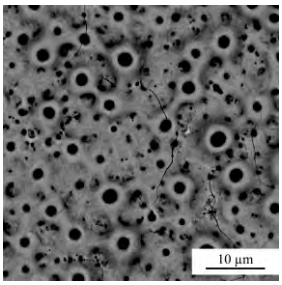

Fig. 4c. Surface morphology of MAO films in electrolytes of different NaOH concentration (NaOH concentration 0.20 mol/L).

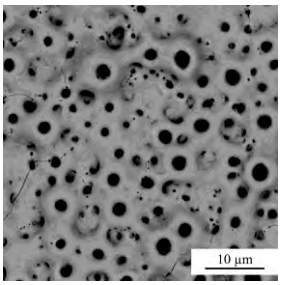

Fig. 4d. Surface morphology of MAO films in electrolytes of different NaOH concentration (NaOH concentration 0.30 mol/L).

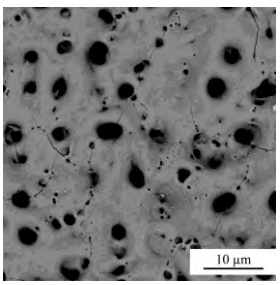

Fig. 4e. Surface morphology of MAO films in electrolytes of different NaOH concentration (NaOH concentration 0.40 mol/L).

crater pores (ruins of the discharge channels). Higher concentration means higher conductivity, which would result in more obvious effect of coating and accumulation as shown in Fig. 4e.

Table 2. The surface roughness of different NaOH concentration

NaOH concentration/mol/L	0.05	0.10	0.20	0.30	0.40
R_z (μm)	0.567	1.225	2.486	1.047	1.776

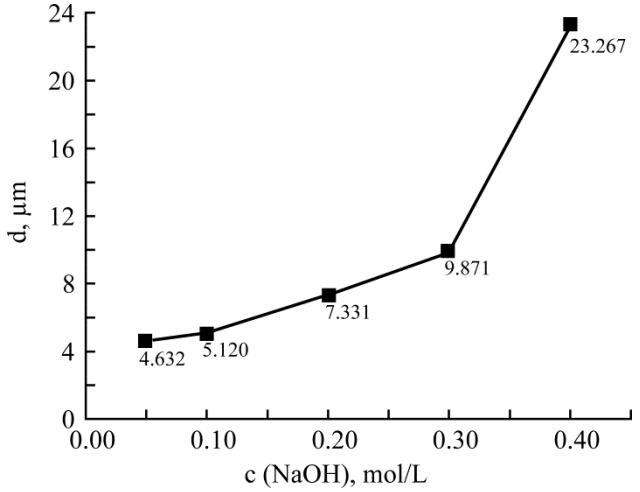

Fig. 5. Dependence of the NaOH concentration on the thickness.

Statistics of MAO coating surface parameters(porosity, pores density & pores size)

After threshold value processing of SEM images (5800×) by digital image software ImageJx2.0, porosity of micro-arc oxidation coating surface was measured according to threshold segmentation principle. The relationship between porosities (PR) and NaOH concentration is shown in Fig. 6. With NaOH concentration increasing, the porosity of micro-arc coating increases, and then decreases. Under 0.10 mol/L, porosity grows up and peaks at 0.10 mol/L with 33.02%; after 0.30 mol/L, the decreasing trend of porosity stops and reaches at 0.40 mol/L with 17.22%. As Eq. 10&11 shown above in section 1.3, when impedance Z keeps stable, electrolyte concentration c and molar conductivity Λ_m have significant correlation with porosity p under the condition that processing time is long enough. When NaOH concentration is under a certain value, the its increasing would promote electrical field that means higher conductivity, which arouses breakdown area's increasing and finally results in higher porosity (Fig. 6). At higher concentration than a certain value, the discharge channels are wider increasingly, and the size of breakdown area increases with the rising of concentration. The metallic melt increased dramatically, accumulated and coated on the surface of substrate, and finally formed the ceramic coating. The coating structures of higher concentrations are irregular, which are not the "fossil" of discharge channels as lower concentration (Fig. 3e and 4c), but are fabricated by the coating and accumulation of massive metallic melt. Thus, in the figure, porosity shows a relatively steady trend with a little decreasing when the concentration is higher than 0.30 mol/L.

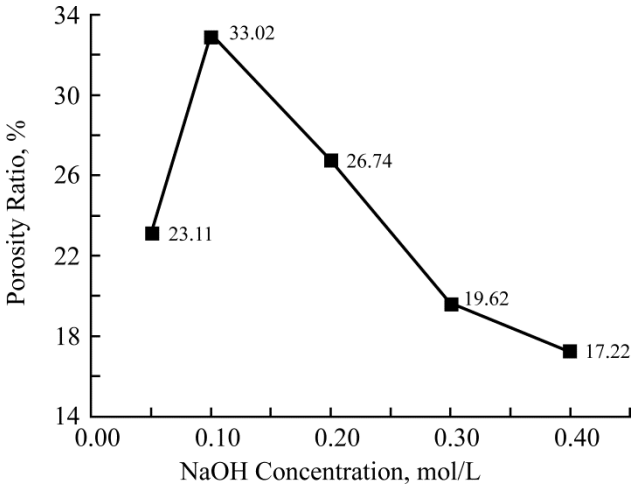

Fig. 6. Effect of different NaOH concentration on porosity ratio.

The dependence of NaOH concentration on pores density (abbreviation is PD, the number of pores per unit area) and the radius of pores (r) were measured which are given in Fig. 7. The two curve lines illustrate that PD decreases, and r rises with NaOH increasing. According to the derivation and analysis of the electrical mathematical interpretation model of MAO process, it is known that this kind of phenomenon in Fig. 7 above can be ascribed to the sharp rise of electrolyte conductivity with NaOH concentration increasing. However, it also indicates that the lack of correlation exists in the field of lower concentration of NaOH between Figs. 6 and 7a. It can be ascribed to the reason as follows: with NaOH concentration increasing, r increases (Fig. 7b), and the PD decreases. From the Eq. 12, the change of r will bring quadratic effect on the porosity compared with the linear effect of PD. On the other hand, r at 0.10 mol/L is about 1.5 times 0.05 mol/L, and the decrease of PD is only about 33%. Therefore, porosity increases and shows irrelevance with PD in lower NaOH concentration. In the higher concentration, the effect of the decrease of PD is much higher than the increase of r, and PD shows correlation with PR.

$$\text{PR} = \text{Porous area/Whole area} = \text{PD} \times (\pi r^2). \quad (12)$$

As shown in Fig. 7a, pore density plays a leading role in deciding the porosity which is current common evaluation standard of Ti alloy biomedical applications such as dental implant. Porosity is the ratio of the area of pores to the whole surface areas as the illustration of Eq. 12. However, appropriate irregular "roughening" of implant surface can enhance the adhesion of implant-bone significantly. Thus, the amount of pores per unit area has important significance in the adhesive strength between

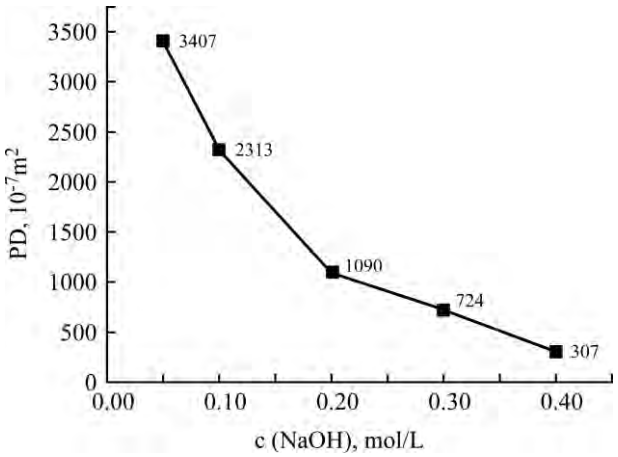

Fig. 7a. Effect of different NaOH concentration on pores density.

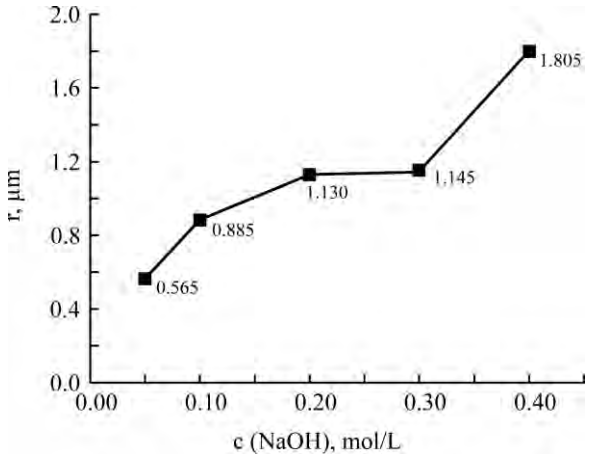

Fig. 7b. Effect of different NaOH concentration on pores size.

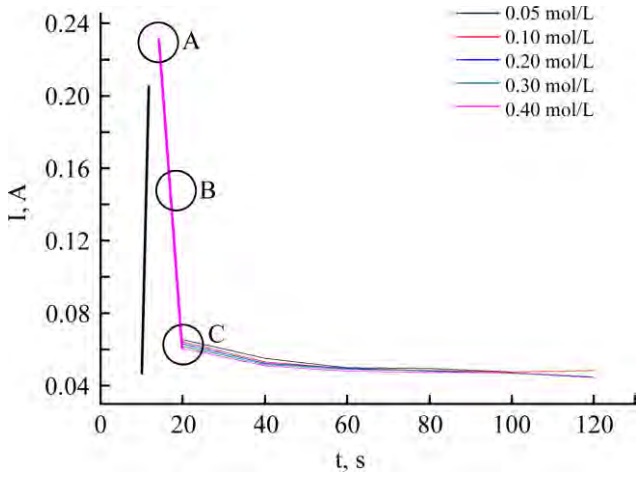

Fig. 8. Relationship between electric current and time.

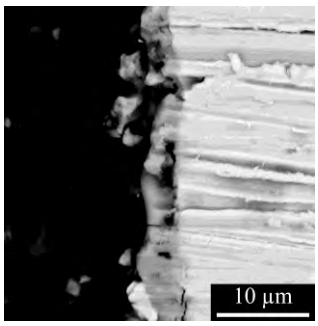

Fig. 9a. The cross-section of MAO coating after treatment 22 s (NaOH: 0.01 mol/L).

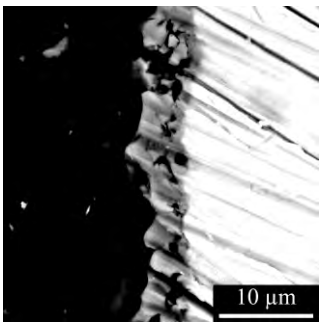

Fig. 9b. The cross-section of MAO coating after treatment 90 s (NaOH: 0.01 mol/L).

Ti alloy and bone issue, and studies and explorations of this aspect were rarely reported unfortunately. How to obtain suitable pores density with conditions that certain porosity is an innovative new direction whose purpose is improving biomedical performance of MAO ceramic coating.

Current response

The current response of MAO process depending on time was shown in Fig. 8. From the diagram, it can be found that current responses of different NaOH concentration have similar trends during the whole process, and the higher concentration current value is higher slightly. Current first increases slowly. After that, it jumps until reaches a peak stage which locates between 12 and 18 s. Then, it decreases significantly to a certain value and keeps around 0.47 A steadily. According to our previous studies, the coating formation process mainly concentrates in the former 40 s from the beginning in power voltage mode which was used in this paper. When time is after 40 s, the thickness and microstructure of MAO coating have no obvious differences and changes (Figure 9).

About the interpretation and explanation of the phenomenon which current keeps stable during the

Fig. 10a. The surface morphology of MAO coating after treatment 5 s (NaOH: 0.02 mol/L).

Fig. 10b. The surface morphology of MAO coating after treatment 14 s (NaOH: 0.02 mol/L).

Fig. 10c. The surface morphology of MAO coating after treatment 17 s (NaOH: 0.02 mol/L).

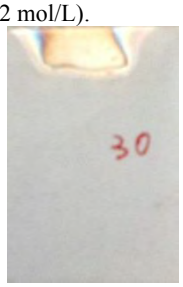

Fig. 10d. The surface morphology of MAO coating after treatment 30 s (NaOH: 0.02 mol/L).

Fig. 10e. The surface morphology of MAO coating after treatment 45 s (NaOH: 0.02 mol/L).

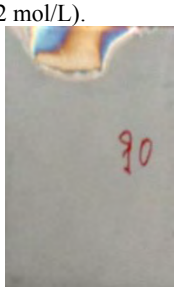

Fig. 10f. The surface morphology of MAO coating after treatment 90 s (NaOH: 0.02 mol/L).

Fig. 10g. The surface morphology of MAO coating after treatment 120 s (NaOH: 0.02 mol/L).

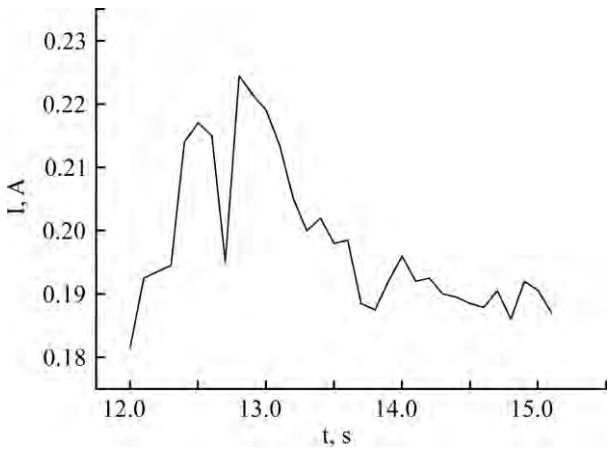

Fig. 11a. The current respond (NaOH concentration: 0.30 mol/L) at point *A*.

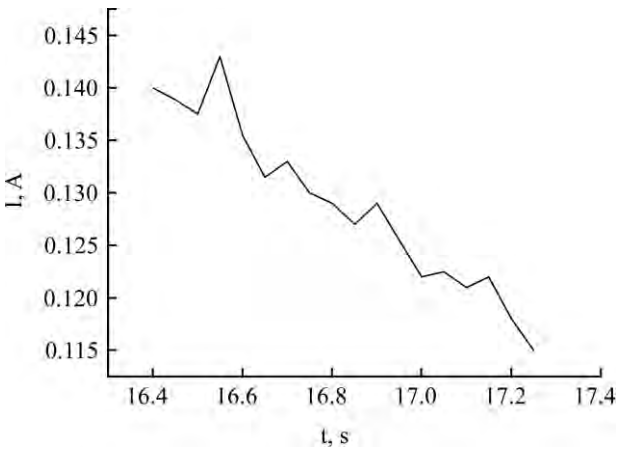

Fig. 11b. The current respond (NaOH concentration: 0.30 mol/L) at point *B*.

latter process, published paper has carried out the detailed elaboration, and current response of AC as shown in the figure was also analyzed in this paper. The maximums of the current response of different NaOH concentration and the AC time lengths were shown in Table 3, it can be seen that the maximum of current response becomes higher increasingly, and the duration of AC is longer with the concentration increasing. Higher electrolyte concentration could increase electrolyte conductivity, which result in the

intense current response. The sample of treatment time 5 s is found that its surface is a layer of anodic oxidation film after observation (Figure 10). However, the sample of 90 s when the current is steady has already been generated MAO coating (Figure 10). Therefore, it can be concluded that the formation of MAO coating was mainly in the process before *A* in Fig. 8. In order to clearly analyzing the current response curves, choosing the 0.30 mol/L curve to be measured particularly, and selecting two significant meaningful curve parts *A* and *B* (Fig. 8) to zoom in as shown in Fig. 11a and 11b.

Table 3. The maximum and length of AC of current respond in different NaOH concentration

NaOH concentration/mol/L	Maximum current/10^{-1}A	Length of time/s
0.05	2.056	6.8
0.10	2.703	7.0
0.20	2.186	7.3
0.30	2.235	7.2
0.40	2.317	7.7

The current response near the maximum (point *A* in Fig. 8) is stable with widespread peaks. Declining curve near point *B* is almost plummeting, and widespread peaks are still existing. There were micro-arcs on the surface of the sample during the whole duration of the experiment process no matter the reaction was intense or not. The speculated reasons are as follows: the generation of micro-arc created the discharge channels and improved the electric field environment, which means that current rose; when the melt generated by micro-arc coated and accumulated on the surface of sample, the discharge channels were blocked, which resulted in the decreasing of current. However, the generation of micro-arc was uncontrollable and irregular. Therefore, irregular spikes appeared in the Figure 9. According to the Eq. 8 & 11, it can be seen that coating thickness is related to electrolyte impendence, voltage and current. In the case with other parameters stable (constant voltage mode), current decreased with the thickness of coating increasing. After the breakdown of oxidation film that the beginning of MAO, the current response was nearly linearity (AC in the figure). The current prediction of the mathematics electrical model established in this paper is accorded with the results of experiment above. In addition, the current response is also influenced by the properties and performance of the supply power so that researchers observed different current response in different papers.

4. CONCLUSIONS

The Ti alloy MAO mathematics electrical model was established in this paper, which includes process parameters (voltage, duty ratio, electrolyte concentration, molar conductivity) and the properties of MAO coating (porosity, pores density, thickness and current response). In the case of the voltage power, NaOH concentration has significant influence on the morphology of the coating surface. When concentration was under 0.30 mol/L, the pores structure of MAO coating was crater shape, and the thickness was linear variation (from 4.632 μm to 9.871 μm). Higher concentration coating was formed by the effect of coating and accumulation, whose thickness was much higher 23.367 μm. Pores density has absolute impact on the porosity, which is also a new pregnant researching area. Current response reached a peak at around 12 ~ 18 s (2.150 A), and there were various spikes during the whole current curve. The formation of MAO coating was before 40 s. The experiment results accords ideally with the model established in this paper under certain NaOH concentration (0.30 mol/L), which provides references to the researchers who focus on micro-arc oxidation.

REFERENCES

1. Wu H.H., Lu X.Y., Long B.H. The Effects of Cathodic and Anodic Voltages on the Characteristics of Porous Nanocrystalline Titania Film Fabricated by Micro-arc Oxidation. *Mater Lett.* 2005, **59,** 370–375.
2. Yerokhin A.L., Nie X., Leyland A. Plasma Electrolysis for Surface Engineering. *Surf Coat Tech.* 1999, **122** (2–3), 73–93.
3. Anusavice K.J., Philips R.W. *Philips' Science of Dental Materials*. 11th ed. St Louis: EIsevier, 2003. pp. 743–53.
4. Yuan-Hong Wang, Zhan-guo Liu, Jia-Hu Ouyang, et al. Preparation and High Temperature Oxidation Resistance of Micro-arc Oxidation Ceramic Coatings Formed on Ti_2AlNb Alloy. *Appl Surf Sci.* 2012, **258**(22), 8946–8952.
5. McKee D.W., Savage R.H., Gunnoe G. Chemical Factors in Carbon Brush Wear. *Wear.* 1972, **22**(2), 193–214.
6. Krishna L.R., Somaraju K.R.C., Sundararajan G. The Tribological Performance of Ultra-hard Ceramic Composite Coatings Obtained Through Micro-arc Oxidation. *Surf Coat Tech.* 2003, **163–164,** 484–490.
7. Yerokhin A.L., Leyland A., Matthews A. Kinetic Aspects of Aluminium Titanate Layer Formation on Titanium Alloys by Plasma Electrolytic Oxidation. *Appl Surf Sci.* 2002, **200**(1–4), 172–184.
8. Dearnley P.A., Dahm K.L., Murakami R. Hard Engineering Surfaces for Aluminium Alloys. *Tribology Series.* 2002, **40,** 1373–1377.
9. Wenbin Xue, Chao Wang, Ruyi Chen, et al. Structure and Properties Characterization of Ceramic Coatings Produced on Ti–6Al–4V Alloy by Micro-arc Oxidation in Aluminate Solution. *Mater Lett.* 2002, **52**(6), 435–441.
10. Tao Zhang, Xiaona Wu, Huayang Huang, et al. The Beneficial Influence of Micro-arc Oxidation-coated Magnesium Alloy on the Adhesion, Proliferation and

Osteogenic Differentiation of Bone Marrow Stromal Cells. *Mater Lett.* 2014, **137,** 362–365.

11. Yonghao Gao, Aleksey Yerokhin, Evgeny Parfenov, et al. Application of Voltage Pulse Transient Analysis during Plasma Electrolytic Oxidation for Assessment of Characteristics and Corrosion Behaviour of Ca- and P-containing Coatings on Magnesium. *Electrochim Acta.* 2014, **149,** 218–230.
12. Khalajabadi S.Z., Kadir M.R.A., Izman S., et al. Effect of Mechanical Alloying on the Phase Evolution, Microstructure and Bio-corrosion Properties of a Mg/HA/TiO_2/MgO Nanocomposite. *Ceram Int.* 2014, **40**(10), 16743–16759.
13. Gu X.N., Li N., Zhou W.R., et al. Corrosion Resistance and Surface Biocompatibility of a Micro-arc Oxidation Coating on a Mg–Ca Alloy. *Acta Biomaterialia*. 2011, **7**(4), 1880–1889.
14. Ho-Jun Song, Kyung-Ha Shin, Min-Suk Kook, et al. Effects of the Electric Conditions of AC-type Micro-arc Oxidation and Hydrothermal Treatment Solution on the Characteristics of Hydroxyapatite Formed on Titanium. *Surf Coat Tech.* 2010, **204**(14), 2273–2278.
15. Malyshev V.N., Zorin K.M. Features of Micro-arc Oxidation Coatings Formation Technology in Slurry Electrolytes. *Appl Surf Sci.* 2007, **254**(5), 1511–1516.
16. Wang Y.M., Wang F.H., Xu M.J., et al. Microstructure and Corrosion Behavior of Coated AZ91 Alloy by Micro-arc Oxidation for Biomedical Application. *Appl Surf Sci.* 2009, **255**(22), 9124–9131.
17. Ikonopisov S. Theory of Electrical Breakdown during Formation of Barrier Anodic Films. *Electrochim Acta.* 1977, **22**(10), 1077–1082.
18. Alebella J.M., Montero I., et al. Electron Injection and Avalanche during the Anodic Oxidation of Tentalum. *J Electrochem Soc.* 1984, **131**(5), 1101–1108.
19. Wen L., Wang Y.M., Zhou Y., et al. Iron-rich Layer Introduced by SMAT and its Effect on Corrosion Resistance and Wear Behavior of 2024 Al Alloy. *Mater Chem Phys.* 2011, **126**(1–20), 301–309.
20. Lee Y.K., Lee K., Jung T. Study on Micro-arc Oxidation of AZ31B Magnesium Alloy in Alkaline Metal Silicate Solution. *Electrochem Commun.* 2006, **10**(1), 1716–1719.
21. Li Hanru. *Introduction to Dielectric Physics*. Chengdu: Chengdu University of Science and Technology Press, 1990. 451 p.
22. Sun Bing. *Discharge Plasma in Liquid and Its Application*. Science Press Beijing, 2013. 251 p.

Received 17.11.14
Accepted 30.12.14

Реферат

Предпринята попытка создания математической модели интерпретации параметров процесса микродугового оксидирования и свойств керамического покрытия в электролитной системе Ca/P. Модель включает в себя параметры процесса микродугового оксидирования (напряжение питания U_m, плотность тока J, скважность η, проводимость электролита и диэлектрическую константу анодного оксида) и свойства керамического покрытия (морфология поверхности, толщина, плотность пор, пористость, средний размер поры). Изучали отклик тока во время процесса. Свойства керамического покрытия (морфология, толщина и статистика поверхности) были определены с помощью сканирующей электронной микроскопии (SEM), видео микроскопа 3-D HIROX, прибора TT230 для измерения покрытия и толщины слоя и программы ImageJx2.0 для анализа изображений. Ток измерялся с помощью гальванометра переменного тока GPM-8212. Молярная проводимость NaOH является самой высокой среди четырех компонентов электролитной системы, и его концентрация имеет наибольшее влияние на морфологию поверхности керамического покрытия. В наибольшей степени анализ согласуется с экспериментальными результатами при его низкой концентрации (до 0,30 моль/л). Тем не менее, есть несоответствие при более высокой концентрации (0,40 моль/л), так как значительно больше образуется расплавленного металла во время реакции МДО в электролите с более высокой проводимостью. Плотность пор является основным фактором, определяющим пористость. Полученные данные показывают, что керамическое покрытие может быть создано в течение 40 секунд в системе с постоянным напряжением. Модель обеспечивает теоретическую базу для интерпретации процесса МАО Ti сплава и определения соответствующей концентрации NaOH в электролитной системе Ca/P.

Ключевые слова: микродуговое оксидирование, сплав титана, математическая модель, Ca/P электролит.